Clay Minerals (2023), **57**, 183–191
doi:10.1180/clm.2022.36

CAMBRIDGE UNIVERSITY PRESS

Article

Geometry optimization of an electrochemical reactor for bleaching kaolin

José Angel Cobos-Murcia[1]*, Eduardo Hernández-Aguilar[2], Ariadna Trujillo-Estrada[1,3], Grisell Gallegos-Ortega[1] and Victor Esteban Reyes-Cruz[1]

[1]Universidad Autónoma del Estado de Hidalgo, Área Académica de Ciencias de la Tierra y Materiales, Carr. Pachuca-Tulancingo km 4.5 s/n, Mineral de la Reforma, Hidalgo, Mexico; [2]Universidad Veracruzana, Facultad de Ciencias Químicas, Ote. 6 1009, Col. Rafael Alvarado, Orizaba, Veracruz, CP 94340, Mexico and [3]Consejo Nacional de Ciencia y Tecnología, Departamento de Cátedras, Av. Insurgentes Sur 1582, Col. Crédito Constructor, Deleg. Benito Juárez, México DF, CP 03940, Mexico

Abstract

High-whiteness kaolinite mining reserves are scarce. In some locations, it is necessary to remove material to access them (adding to the cost). Therefore, processes have been developed to eliminate contaminants, such as iron, and provide alternatives to the used contaminated materials that, after being treated, meet quality criteria. In our previous research, we developed an electrochemical process for kaolin whitening at the laboratory level and bench scale, demonstrating the reaction mechanisms that occur during the removal of iron from kaolin. However, the geometry used at the laboratory level does not present the most suitable position for the electrodes. Therefore, in the present study, we focused on the geometry and the function of the electrodes. This is necessary during the escalation process to reach the pilot-scale level. The study was carried out using computer-aided engineering in the *COMSOL Multiphysics* computer program and by analysing the distribution of the electric potential and the electric current of the geometries considered while performing the scaling. The results indicated that the change in the anode position from perpendicular to parallel to the discs improved the distribution of electric current density on the cathode surface and so increased the elimination of iron through electrochemical deposition. Similarly, to reduce the amount of material used in the construction of the reactor, the anode-size effect was analysed, revealing that relatively small anodes improved the distribution of electric current density over the entire surface of the electrode and not only at the edges.

Keywords: bleaching, distribution of electric current density, electrochemical reactor, kaolin, simulation

(Received 19 August 2022; revised 18 November 2022; Associate Editor: Chun Hui Zhou)

High-purity white kaolin mining reserves have become increasingly scarce. Therefore, processes have been developed to remove the contaminants from kaolin, such as sulfur, titanium, iron and heavy metals, among others. These impurities give kaolin undesirable properties for the ceramics, paper, paint, food and pharmaceutical industries: pollutants favour cavitation in the ceramic process, increase hardness, cause abrasion and give kaolin various shades of colour from off-white to red.

Treatment processes focus on eliminating these contaminants in addition to quartz. The main methods for bleaching kaolinite are wet treatments, such as flocculation with polymers, chemical solubilization, extraction and washing (Bloodworth *et al.*, 1993).

Therefore, new methodologies have been developed for the removal of these contaminants (Bloodworth *et al.*, 1993; Li *et al.*, 2013), such as flotation (Maynard *et al.*, 1969; Raghavan *et al.*, 2004), chemical treatment by chlorination (González & Ruiz, 2006), treatments with inorganic acids (Hernández-Hernández *et al.*, 2015), organic acids (Ma & Li, 2006), organic bases (Pentrák *et al.*, 2018) and reducing agents (Panzhong *et al.*, 2010), microbiological treatments (Shelobolina *et al.*, 2005), thermal processes (Chen *et al.*, 2014), magnetic methods (Li *et al.*, 2013) and electrochemical techniques (Lu *et al.*, 2006; Flores-Segura *et al.*, 2012).

Note that the apparatus for the kaolin-whitening process was registered in intellectual property offices in 1806 (Langenbeck, 1908). Only mechanical treatment and separation processes were considered to generate adequate particle sizes. Chemical treatments were later incorporated, including washes in water and hydrogen sulfide to separate contaminants such as iron sulfide from kaolin. The most commonly used technologies include the chemical processes of whitening kaolin (Forbus *et al.*, 1993; Yildirim *et al.*, 2012; Yin & Huang, 2013; Li, 2014; Wang *et al.*, 2021), chemical–heat treatment (Shengwu *et al.*, 2012; Yijun *et al.*, 2012), thermal methods (Berube *et al.*, 1990), use of ion-exchange resins in solution (Thompson, 1982) and exchange columns (Yishui *et al.*, 1989).

Our research group developed a kaolin-whitening technology (Flores-Segura *et al.*, 2017) which uses an electrochemical technique and has filed for a patent (Reyes-Cruz & Flores-Segura, 2015). Thus far, this technique has been applied to kaolinites of various origins, such as Veracruz, Hidalgo and Michoacan,

*Email: jose_cobos@uaeh.edu.mx

Cite this article: Cobos-Murcia JA, Hernández-Aguilar E, Trujillo-Estrada A, Gallegos-Ortega G, Reyes-Cruz VE (2023). Geometry optimization of an electrochemical reactor for bleaching kaolin. *Clay Minerals* **57**, 183–191. https://doi.org/10.1180/clm.2022.36

which have the most important reserves and greatest variety in Mexico, considering the various concentrations of polluting iron producing kaolinites with whiteness indices of between 70 and 90 (Reyes-Cruz & Flores-Segura, 2015; Flores-Segura *et al.*, 2016, Melo-López *et al.*, 2018).

Furthermore, the process of iron mass transfer towards the electrode surface (Flores-Segura *et al.*, 2016), the use of various dispersants (Reyes-Cruz & Flores-Segura, 2015) and the effect of applying ultrasound waves during the whitening process have been studied (Melo-López *et al.*, 2018). The kaolin-whitening technology has been negotiated with companies interested in its application in Mexico, and bench-scale and pilot-scale tests have been conducted under natural conditions as part of the technology transfer of the recent patent filing for the apparatus for bleaching kaolin (Reyes-Cruz *et al.*, 2017). The industry's interest in this technology is attributed to the potential competitive advantages it could bring, such as the specificity of magnetic bleaching, which is set by the fraction of the iron present as a contaminant; the use of fewer reagents than chemical bleaching; and the high costs of ion-exchange processes. However, the technology is still being adapted and conditioned under real operating system conditions.

Therefore, for the reactor-scale process of the device, the geometry, operating conditions, cost and quantity of materials have been evaluated (Nadebaum & Fahidy, 1980; Walsh & Reade, 1994). An electrochemical reactor was also used to assess factors such as the electrochemical potential and the electric current limit (Houghton & Kuhn, 1974; White *et al.*, 1983; Bisang & Kreysa, 1988; Li, 2017) as well as the distribution of both of these factors, which allowed for reductions in manufacturing costs to be realized (Nadebaum & Fahidy, 1980; Sulaymon & Abbar, 2012). Such work improved the removal of iron and so the whiteness of the kaolin obtained.

Computer-assisted engineering using numerical methods is a helpful tool for studying the geometry of electrochemical reactors (Rodríguez-Morales *et al.*, 2020). In some cases, the contribution of mass transport can be ignored (Liu *et al.*, 2004) to optimize geometries and the position of the electrodes and the separators (Lee & Selman, 1982). In addition, a numerical analysis has been conducted to study the behaviour of kaolinite during treatments for electrokinetic remediation. The transport of pollutants through solid kaolin has been studied using various gradients of the electric potential (Yustres *et al.*, 2018). Fluid dynamics in separator hydro-cyclones have also been analysed, which has improved our understanding of the transport and separation mechanisms of the contaminating particles (Cullivan *et al.*, 2003). Note that the hydro-cyclone has been the most studied purification process (Lim *et al.*, 2010). A separation study has also been carried out using magnetic gradients and analysing the diffusion of pollutant particles (Okada *et al.*, 2007). The flash-calcination process has also been simulated in which the temperature and time values were optimized to avoid the conversion of kaolin to metakaolin (Teklay *et al.*, 2016).

Therefore, this work focused on geometrical aspects, and the electrode array was denoted in this work by modelling the distribution of the electric current and the electric potential. The use of computational tools to justify the geometry change was done with the aim of increasing the amount of electrochemically deposited iron and at improving the bleaching process. In this regard, studying the position and the size of the electrodes used could enable us to use the least amount of material possible to construct such a reactor. Some companies in Mexico are particularly interested in this technology as the reserves of white kaolin are in shorter supply at present than the reserves of kaolin that have contaminants such as iron. The electrochemical bleaching technology developed is currently at a technology readiness level of 7 and has significant potential for industrial applications.

Materials and methods

Geometry studied

As is shown in Fig. 1, two geometries were evaluated to assess the effect of geometry on the electric current and the electric potential distribution. The geometry in Fig. 1a denotes the original geometry of the device, which has circular cathodes with diameters of 30 cm and thicknesses of 3 mm. The anodes had widths of 20 cm and thicknesses of 2.5 cm. Figure 1b shows the proposed geometry in which the anodes were placed between the cathode discs; it also presents the dimensions of the anodes. Finally, Fig. 1c shows the geometry assessed with the anodes in a parallel position to the cathodes and with the anodes having square geometries of 10, 20 or 30 cm.

Mathematical model

The electrochemical reaction on the electrodes is considered reversible (Pérez *et al.*, 2015) because there is no accumulation of charges in the electrolyte and the concentration gradient is negligible. Hence, uniform conductivity occurs in the electrolyte and at the electrodes. Therefore, it is possible to consider that the primary distribution of electric current density depends only on the geometry of the reactor (Vázquez *et al.*, 2012), and the general flow equation can be expressed as in Equation 1:

$$\frac{\partial^2 \varphi}{\partial x^2} + \frac{\partial^2 \varphi}{\partial y^2} + \frac{\partial^2 \varphi}{\partial z^2} = 0 \tag{1}$$

where φ is the electric potential in the electrolyte concerning the geometrical coordinates, and the distribution of electric current density considers that both the load transfer and the mass transport conditions are negligible because the ohmic resistance inside the cell determines the distribution of electric current density. Thus, it is possible to set the electric current values at any reactor coordinates. For the present study, the above considerations allow us to assume that it is possible to establish the distribution of electric current density in the electrolyte inside the reactor.

The primary and secondary distribution of electric current density simulations were performed considering the data presented in Table 1 under stationery and convection conditions. These conditions were established through the experimental conditions obtained during the kaolin-bleaching process at the laboratory level (Melo-López *et al.*, 2018).

The electric current density (j) was determined at any point in the reactor according to Ohm's law by the local electric potential gradient, where k is the conductivity of the electrolyte, which describes the distribution of the electric current and potential in the electrolyte, depending on the electrochemical potential imposed on the reactor (Equation 2). This is calculated throughout the geometry using the Laplacian operator (∇) on the function that represents the electric potential (φ) as a scalar field:

$$j = -k\nabla\varphi \tag{2}$$

https://doi.org/10.1180/clm.2022.36 Published online by Cambridge University Press

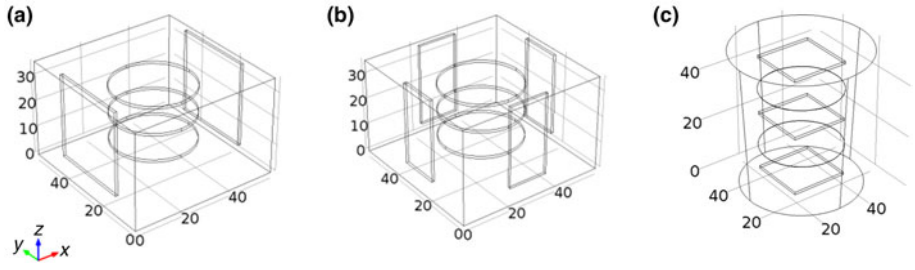

Fig. 1. Geometries that were evaluated to improve the distribution of electric current density. (a) Original design with two perpendicular anodes. (b) First proposal with four perpendicular anodes. (c) Second proposal with parallel anodes of 10, 20 or 30 cm.

Table 1. Parameters used in the numerical simulation.

Parameter	Value
Electrolyte conductivity (k; S m^{-1})	0.02
Cathodic Tafel slope (b_c; V)	–0.118
Anodic Tafel slope (b_c; V)	0.118
Cathodic electrochemical overpotential (η_c; V)	–2
Anodic electrochemical overpotential (η_a; V)	2
Cathodic transfer coefficient (α_c)	0.1
Anodic transfer coefficient (α_a)	0.9
Exchange in electric current density (i_0; A)	2.4
Temperature (T; K)	293.15

In addition, the other walls that were not electrodes were considered to be insulating, and so no electric current flow occurred; here, ξ denotes the typical surface condition (Equation 3). In the case of the kaolin-bleaching reactor, this mainly represents the walls that contain the kaolin emulsion to be bleached but that do not participate in the electronic exchange.

$$-k\frac{\partial\varphi}{\partial\xi}=0 \tag{3}$$

In contrast, processes that depended on electronic transfer, such as conditions in the electrodes and the electrochemical reaction on the electrode, were considered only in the secondary distribution because the charge transfer and the concentration gradient were considered negligible during the reactor operation.

Therefore, species concentrations were similar at the electrode–electrolyte interface and in the electrolyte bulk. The electric current density was determined from the local electrochemical overpotential in the electrode (η), which is expressed as the difference between the imposed electrochemical potential (E_{imp}) and the electric potential of the solution at the interfacing electrode (φ), as in Equation 4:

$$\eta = E_{imp} - \varphi \tag{4}$$

Accordingly, the Tafel approximation determines the magnitude of the electric current density. Here, j_0 is the exchange electric current density and b_c is the Tafel slope (Equation 5), which is associated with the amount of iron deposited on the cathode surface and, therefore, was removed from the kaolin emulsion.

$$j = j_0\exp\left(\frac{-\eta}{b_c}\right) \tag{5}$$

Under controlled charge-transfer conditions, the electrochemical reaction followed Tafel kinetics on the working electrode (Equation 6). This condition was possible for the reactor operation as the process was carried out *via* forced convection through rotating-disc electrodes.

$$-k\frac{\partial\varphi}{\partial\xi} = -j_0\exp\left(\frac{-\eta}{b_c}\right) \tag{6}$$

Moreover, the electric current density applied at the anode was considered constant (Equation 7) as the reactions on the anode surface were mainly the hydrolysis of water for the evolution of oxygen:

$$-k\frac{\partial\varphi}{\partial\xi} = -j_{ave}\exp\left(\frac{A_c}{A_a}\right) \tag{7}$$

where j_{ave} is the average electric current density at the cathode and A_c and A_a are the area of the cathode and the area of the anode, respectively. Obtaining the area and positions of the electrodes was the objective of the evaluation using numerical methods to improve the distribution of electric current density in the geometry of the reactor.

The average electric current density was the same as the electric current applied between the cathode and the anode. However, the distribution of electric current density was not uniform even when the anode electric current was considered constant. Moreover, the changes in the distribution of electric current density at the cathode were negligible (Low *et al.*, 2007). Therefore, simplifying the boundary condition allowed us to maintain a fixed electric current density at the cathode (Pérez *et al.*, 2015). Thus, the average electric current density could be calculated using Equation 8, with the electric current imposed between the cathode and the anode:

$$j_{ave} = \frac{1}{A_c}\int_0^{A_c} j_{ave}\mathrm{d}A_c \tag{8}$$

Note that the present study aimed to improve the operation of the reactor by optimizing the geometry and position of the electrode. The concentration of iron on the surface electrode was constant because of the convection contribution caused by the rotation of the electrode, as this maintained a constant angular velocity and allowed laminar flow to occur.

Simulation

The theoretical analysis of the primary distribution of the electric current and the potential of the geometries sketched (Fig. 1) was carried out using an approximation of the Laplace equation (Equation 2) at any point inside the reactor; the approximation was determined from the gradient of the local electric potential

https://doi.org/10.1180/clm.2022.36 Published online by Cambridge University Press

using the software *COMSOL Multiphysics*® 3.5 in a WorkStation Dell® Inspiron 20 model 3048 series with Intel® Xeon™ Silver 4116 and two processors with 2.10 GHz and 256 GB of RAM. For this analysis, a mesh was constructed that considered the geometry of the electrode, including $\sim 6 \times 10^5$ total elements and 3.7×10^4 contour elements.

The analysis was carried out to determine how many electrodes the reactor needed. First, this value was obtained with two electrodes (Fig. 1a) according to the original design and the first proposal, and then using the second design with four electrodes (Fig. 1b), the latter electrodes being half the size of the electrodes in the two-electrode array.

However, this first proposal only reduced the amount of material necessary for the construction of the reactor. Therefore, the position changes of the anode were evaluated using a parallel cathode instead of the original perpendicular cathode position. Similarly, the effect of anode size was analysed by considering anodes with square geometries of 10, 20 or 30 cm (Fig. 1c).

Experimental validation

The kaolinite suspension was prepared using 30 kg of kaolin in 230 L of drinking water. Subsequently, oxalic acid ($H_2C_2O_4$) at 1 M and 0.5 kg of sodium silicate were added at a concentration of 0.45% (m/v) as a dispersant to improve the homogeneity of the suspension, and the solution was stirred at 800 rpm for 30 min using the cathodes (rotary disc) of the same apparatus to promote the hydrodynamic force.

A suspension of kaolin was used as the electrolyte. The electrodes were connected to a power supply, namely BK Precision model 1796, while two multimeters were connected between the power supply and the reactor to measure the electric current and the cell electric potential of the reactor. To verify the results obtained through the simulation, a prototype reactor was used for the whitening process with the geometry changes obtained from the simulation, for which discs were used as anodes with diameters of 30 cm. Furthermore, a power source was used in a two-electrode arrangement, imposing on the reactor a constant cell electric potential of 4 V, and we recorded the electric current values obtained. The electric potential imposed was established according to the results of Flores-Segura *et al.* (2017) under laboratory conditions and during the escalation process as expressed in the registered patent. The electrochemical system consisted of four brass discs with diameters of 30 cm each as the cathodes and four graphite sheets of 30 cm per side and 1" thickness as the anodes.

The X-ray diffraction (XRD) analyses of the treated kaolin were carried out in an Inel model Equinox 2000 instrument with a cobalt source. Whiteness was measured using an Ocean Optics USB 4000 spectrometer and conductivity was measured using an ORION Thermo Scientific-brand potentiometer using a 013010MD conductivity cell. In addition, deposits on the surfaces of the cathodes were compared between the perpendicular and the parallel arrays using the image analysis software *OriginPro 2022* version 9.9, which generated an image profile plot for the image data analysis. The image data were transformed into greyscale images or 8-bit colour images, and the minimum and maximum values for each bit of the image were determined and recorded within a matrix; a radial line was selected for the deposit thickness analysis. Finally, the data profile obtained was normalized and compared.

Results and discussion

Number of anodes in a perpendicular position

At the laboratory level, the reactor only had a single disc as the cathode and one or two plates as the anodes, placed on the sides of the reactor (Fig. 2a), whose geometry was analysed. Therefore, to improve the efficiency of the process at the pilot plant level, it was necessary to evaluate other geometries because the distribution of electric current density (Equation 1) affected directly the quantity of iron deposited on the electrode and, thus, the whitening process.

Therefore, the following was evaluated as the first alternative: a reactor with four relatively small-dimension electrodes. Figure 2 compares the distributions of electric current density in the electrolyte and on the surface of the appliance when using arrangements of two (Fig. 2a,b) or four (Fig. 2c,d) electrodes in the perpendicular position.

The distribution of electric current density was direct only near the cathode and the anode. Thus, the most significant distribution of electric current density of the electrolytic solution was found on the edges of the discs (Fig. 2a) with values of $\sim$0.06 mA cm^{-2}, and the rest of the surface disc only had values of $\sim$0.02 mA cm^{-2}.

The most significant distribution of electric current density on the contour disc was observed and was presented as the tangent line of the cathode disc facing the anode (Fig. 2b). While on the sides, where it did not meet the anode, the distribution of electric current density was <10%. Thus, the distribution of electric current density on the anode (Fig. 2b) showed that the maximum distribution of electric current density occurred on the upper edge of the electrode compared to the central electrode region; the distribution of electric current density was $\sim$75% at the upper edge of the electrode, with an distribution of electric current density of 0.04 mA cm^{-2}. While on the sides, the distribution of electric current density was <0.01 mA cm^{-2}, as was reported experimentally previously (Melo-Lopez *et al.*, 2018).

The best distribution of electric current density of the cathode in this cross-section was observed in front of the anode. The distribution of electric current density decreased with increasing distance from the cathode until its value reached 5% on the sides. In addition, the anode demonstrated that its lateral and central regions were more extensive than the distribution of electric current density because of the cathode geometry effect. However, the distribution of electric current density was homogeneous, exceeding a value of 85% over almost the entire electrode length.

In contrast, in the analysis of the geometry with a pair of lateral electrodes, the non-homogeneous distribution of electric current density affected the efficiency of the reactor. Therefore, a change in geometry from the first proposal was considered by placing four separate anodes at every 90° with respect to the disc axis (Fig. 2c). However, to prevent construction costs from increasing, the width of the anodes had to be half of the value for this anode dimension in the first array with two anodes.

The distribution of electric current density in the electrolyte (Fig. 2c) was homogeneous, with values of $\sim$0.06 mA cm^{-2} at the periphery of the cathodes and reaching 0.08 mA cm^{-2} in the region near the anodes. The distribution of electric current density on the disc (Fig. 2d) showed that the distribution of electric current density had values of >70% of the electric current over the entire periphery of the electrode. This was in contrast to the findings for the array with two electrodes, where only half of the edge of the disc presented such high values. Note that the

https://doi.org/10.1180/clm.2022.36 Published online by Cambridge University Press

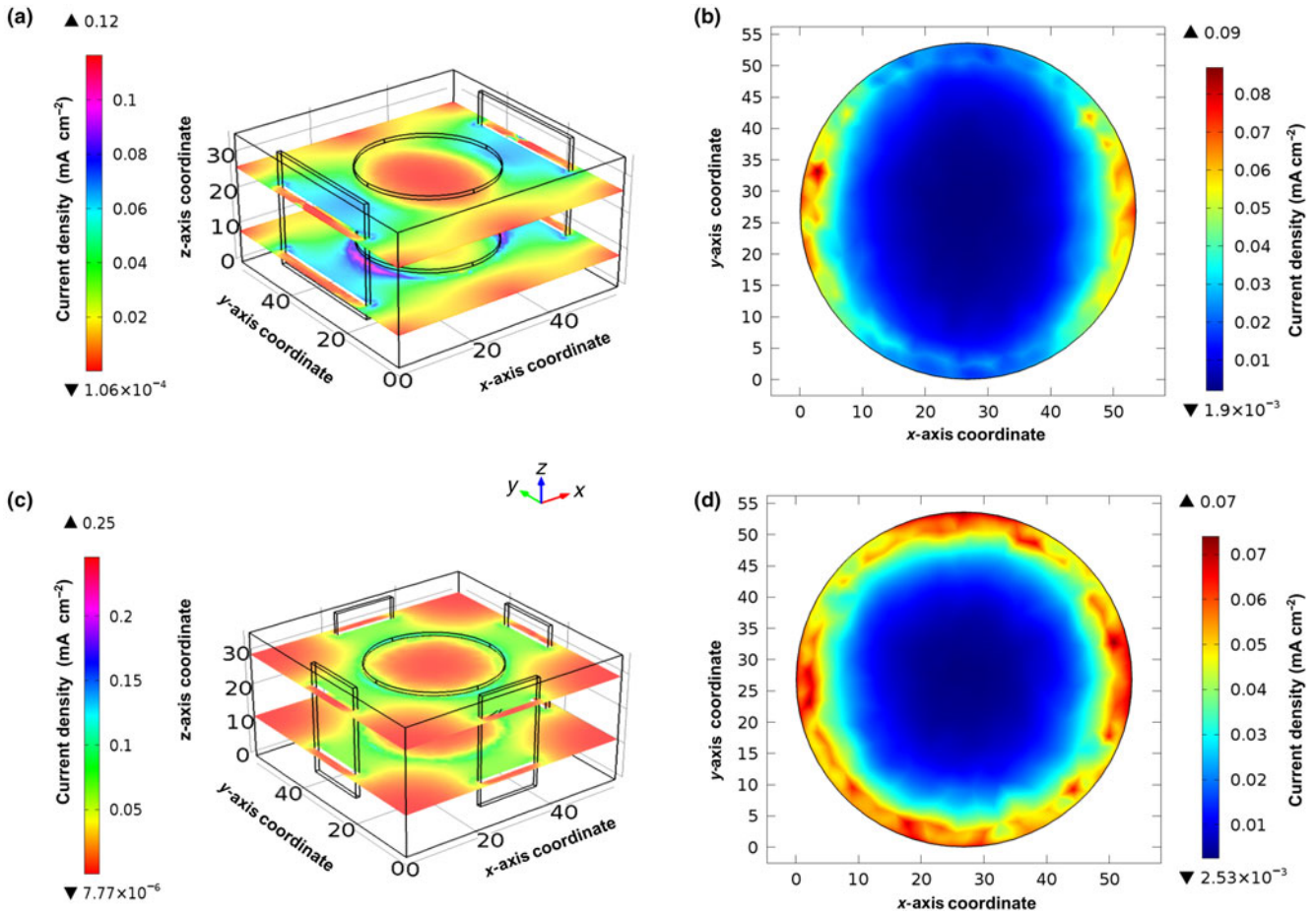

Fig. 2. Geometry with four anodes in a perpendicular position. (a) Surface of the distribution of electric current density and surface of arrows of electric current density in the *x*–*z* plane. (b) Surface of the electric distribution of electric current density in the *x*–*z* plane. (c) Normalized distribution of the upper and lower walls of the cathodes in the *x*–*z* plane. (d) Normalized distribution of the anode wall in the *x*–*z* plane.

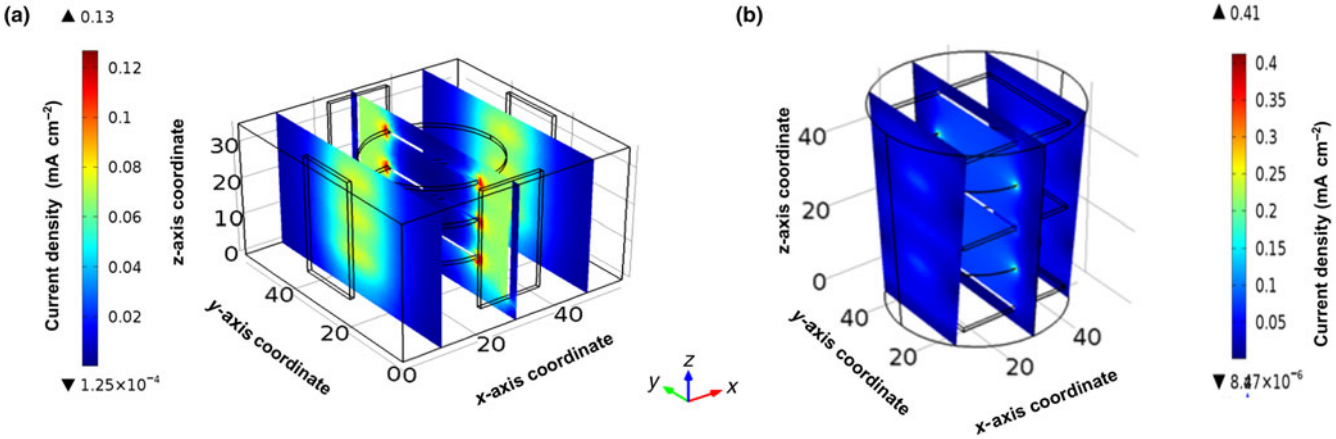

Fig. 3. Section cutting the *x*–*z* plane of the distribution of electric current density in the electrolyte using (a) the array with four anodes in a perpendicular position and (b) the array with anode electrodes in parallel.

distribution of electric current density on the anode was less than that when using two electrodes because of the decrease in the anode width; however, the distribution of electric current density of this four-anode array over the entire surface exceeded that of the two-anode array by 74%.

The results indicated that the use of four anodes could improve the distribution of electric current density. This affected the quantity of iron deposited on the cathode and the whitening process (Equation 2). In the case of the four-anode array, the electric current density doubled, achieving maximum values of 0.12 mA cm^{-2}

https://doi.org/10.1180/clm.2022.36 Published online by Cambridge University Press

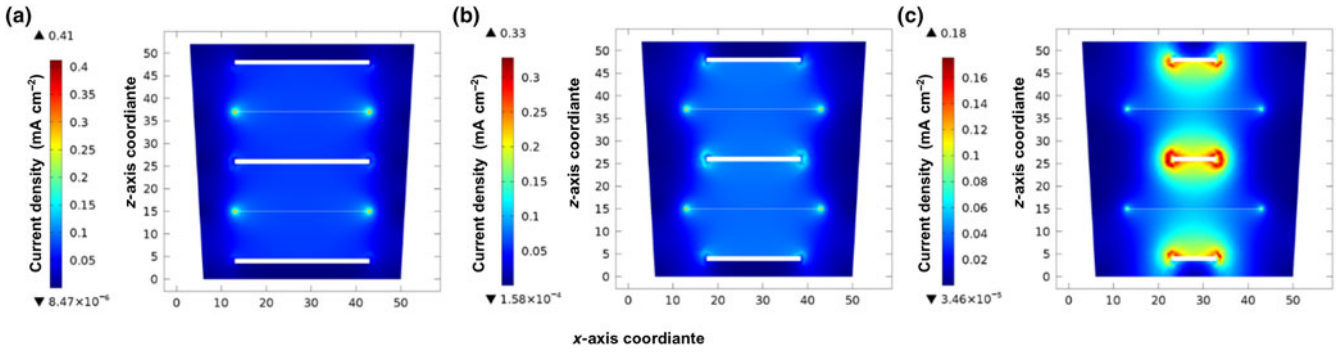

Fig. 4. Section cutting the *x*–*z* plane of the distribution of electric current density in the electrolyte using anode sizes of (a) 30 cm, (b) 20 cm and (c) 10 cm.

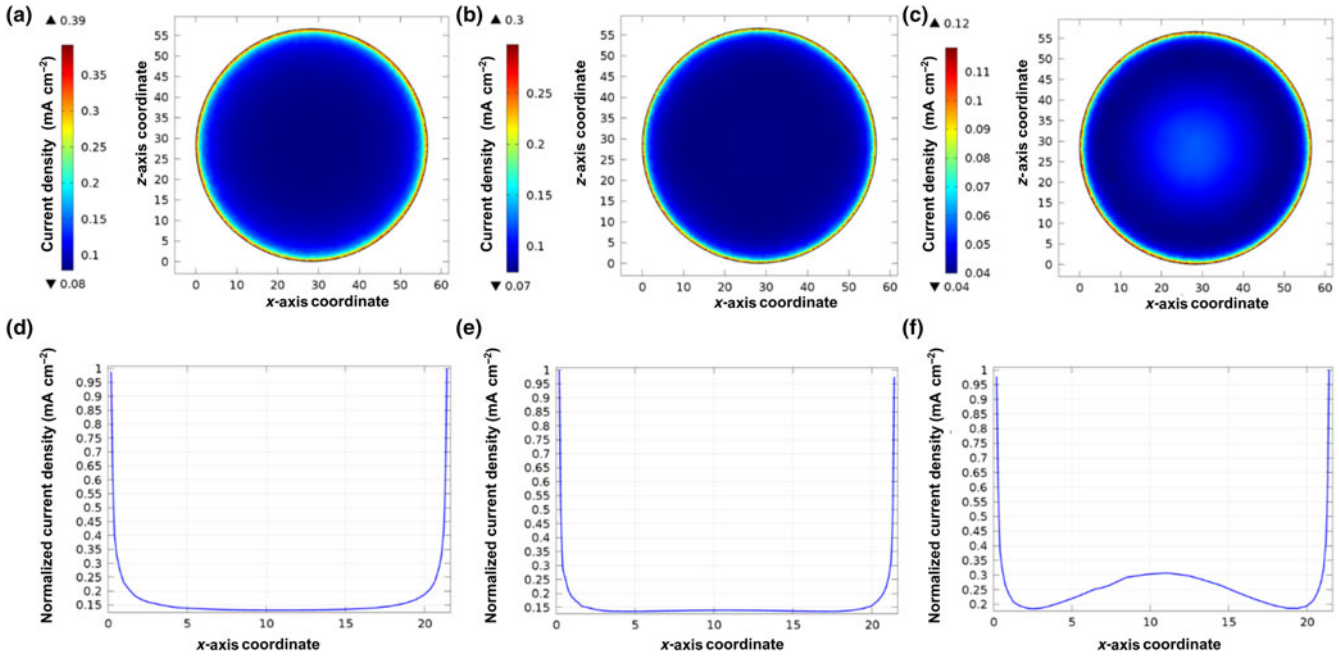

Fig. 5. Distribution of electric current density over the cathode using three different anode sizes: (a) 30 cm, (b) 20 cm and (c) 10 cm. Normalized distribution of electric current density of the diametral line of the cathodes using three different anode sizes: (d) 30 cm, (e) 20 cm and (f) 10 cm.

at the periphery of the discs and 0.02 mA cm^{-2} at their centre. However, we observed that the centre of the discs had low distributions of electric current density. In contrast, in the case of two anodes, the distribution of electric current density was mainly focused at the sides of the two discs, whereas in the case of an array with four anodes the distribution of electric current density was increased at the cathode, thereby improving the distribution of electric current density in the other electrode regions and the electric current penetration into the disc.

Change of anode position: from a perpendicular to a parallel array

The effect of the anode position in the electrode array was analysed (Fig. 3) using anodes in perpendicular (Fig. 3a) and parallel (Fig. 3b) positions.

The distribution of electric current density was more homogeneous in the parallel than the perpendicular anode arrays; therefore, the distribution in the electrolyte improved significantly with a change in the anode position from perpendicular to parallel because of the closer proximity of the electrodes and their greater surface area, leading to increased amounts of iron deposited. These arrays showed an average distribution of electric current density in the electrolyte of 0.1 mA cm^{-2}, with great values observed in regions near the edges of the discs. Some of the recorded values of ~0.2 mA cm^{-2} were double those observed in the same parts of the perpendicular array.

However, this array had certain disadvantages because of the number of anodes required, increasing reactor construction costs. Thus, the size of the anodes was evaluated in the parallel array to analyses its effect on the distribution of electric current density.

Effect of anode size

A cut in the *x*–*z* plane of the distribution of electric current density within the electrolyte was analysed for three different anode sizes: 30 cm (Fig. 4a), 20 cm (Fig. 4b) and 10 cm (Fig. 4c). The distribution of electric current density was more significant at the edges of the anode as the size of the anode increased.

https://doi.org/10.1180/clm.2022.36 Published online by Cambridge University Press

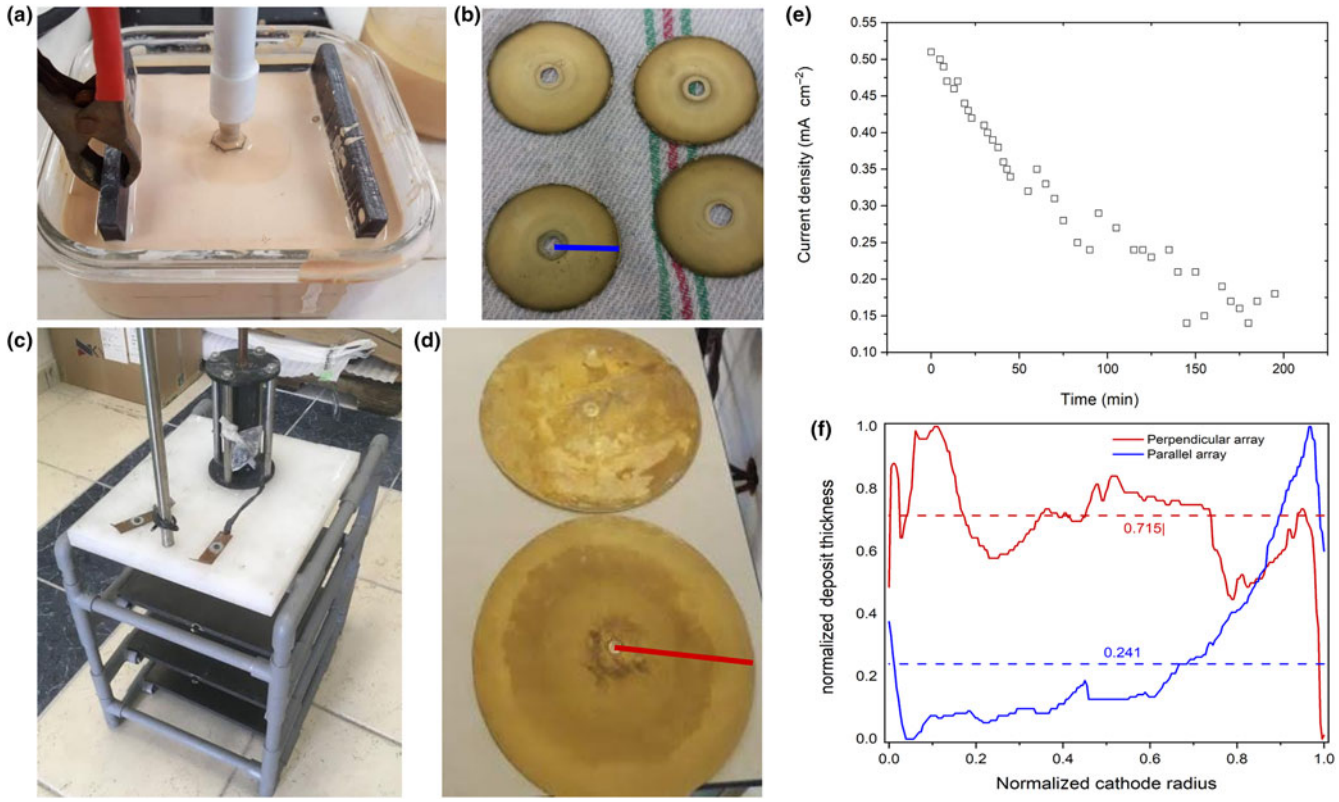

Fig. 6. Validation of electrochemical iron deposits using the cells (a) at the bench-scale level with (b) their respective 7-cm diameter electrodes and (c) at the pilot-scale level with (d) their respective 30 cm-diameter anodes. (e) Chronoamperometry using 30 cm discs and (f) evaluation of the coating *via* image analysis of the perpendicular and parallel arrays.

When the anode size decreased, the electric current density was concentrated at the centre of the reactor, decreasing the electric current density at the edges of the cathodes, and the electric current density near the anode reached values of 0.16 mA cm^{-2}. In contrast, the electrolyte regions near the cathode were homogeneous, although there were still regions with greater distributions on the cathodes.

The distribution of electric current density on the cathode surface (Fig. 5) was analysed using the same three different anode sizes: 30 cm (Fig. 5a), 20 cm (Fig. 5b) and 10 cm (Fig. 5c). The cathode showed a greater electric current density at the disc edge (0.35 mA cm^{-2}) and a lower electric current density at the centre (0.10 mA cm^{-2}) when the anode size decreased.

However, near the anode the electric current density reached 0.16 mA cm^{-2}, but near the cathode the distribution of electric current density was more homogeneous. The more extensive anode distribution showed maximum values of the distribution of electric current density at the edges and a value of 0.15 mA cm^{-2} at the centre of the disc. Therefore, as the anode dimensions decreased, the distribution increased at the centre of the disc, reaching average values of 25%.

Validation of results by evaluation of the metal deposits

On the basis of the distribution of electric current density results, we could propose improvements to the construction of a pilot-scale reactor by relying on these results to understand behaviour at the electrode surface and not only on the empirical knowledge of the behaviour of the electrochemical system or conjectures regarding the distribution of electric current density in the reactor. The reactors (Fig. 6) at the bench-scale level (Fig. 6a) with 7 cm-diameter electrodes (Fig. 6b) and at the pilot-scale level (Fig. 6c) with 30 cm-diameter anodes (Fig. 6d) were analysed. Furthermore, chronoamperometry was conducted using 30 cm discs (Fig. 6e), and the coating was evaluated through image analysis of the perpendicular and parallel arrays (Fig. 6f).

The metallic deposit obtained in the laboratory electrochemical cell (Fig. 6b) was thicker at the edge of the disc, displaying the characteristic burn described in electroplating. In contrast, the metallic deposit obtained in the pilot plant (Fig. 6d) was distributed over the entire electrode surface and was proportional to the distribution of electric current density on the surface of the electrode.

The observed burning zone was associated with a great electric current density in the disc region because of its proximity to the anode and the high rate of iron consumption in this region of the disc. The concomitant increase in the rate of reaction resulted in typically disordered and porous deposits. However, a geometry change was implemented during reactor scaling that prevented the occurrence of an inadequate distribution of electric current density and improved the operation of the reactor.

The electric current density curve obtained using the prototype (Fig. 6e) of the electrochemical reactor in a two-electrode arrangement and using a brass disc as a cathode and a graphite plate as an anode was plotted. An electric current density of 0.45 mA cm^{-1} was reached. This decreased with the modification of the electrode surface until stabilization after 2 h of operation, at which point an average electric current density of 0.15 mA cm^{-1} was reached. The modification of the cathode surface generated a change in the electrochemical reduction potential of the metal and affected

https://doi.org/10.1180/clm.2022.36 Published online by Cambridge University Press

Table 2. Chemical characterization of kaolin before and after treatment using the electrochemical reactor.

Parameter	Before	After
$Al_2H_4O_9Si_2$ (%)	76.2	78.1
TiO_2 (%)	7.0	8.9
CrO_2 (%)	10.0	6.7
Fe_2O_3 (%)	6.0	6.5
Whiteness (a.u.)	79.7	82.5

the amount of iron deposited, which was evidenced by the decrease in the electric current density. Therefore, it was necessary to change the cathode or to clean it to refresh its brass surface.

An evaluation of the coating through image analysis (Fig. 6f) of the perpendicular and parallel arrays was carried out. The effect of the geometry of the reactor could be observed as the parallel arrangement of electrodes produced a better distribution of the deposit, which was associated with the distribution of the electric current density on the surface. This represented greater availability of the surface for the recovery of the contaminant, thereby improving the efficiency of the process of kaolin purification, as it was possible to increase the amount of iron removed.

Finally, the effect of the treatment was observed in the decrease of the iron concentration in kaolin (Table 2) and as shown by the chemical characterization results using XRD (data not shown). Similarly, an increase in whiteness after the electrochemical treatment was observed. Note that the process still needs to be optimized in terms of the concentrations of reagents and operation times to improve the whitening of kaolin.

Conclusion

The computational simulation revealed that the geometry of the electrode array of the electrochemical reactor was improved through visualizing the distribution of electric current density. It was possible to demonstrate that a parallel electrode array had a greater distribution of electric current density. In contrast, it was determined that the use of relatively small electrodes would not affect the distribution of electric current density at the electrode edges and would improve the distribution of electric current density at the centre of the disc. It was also necessary to avoid increasing the amounts of materials used to construct the reactor so as to limit construction costs. We achieved a distribution of electric current density of >20% over the entire surface, and regions in the electrode centre had a distribution of electric current density of ∼30%. The validation of the deposition process showed that the metallic deposits obtained during start-up and evaluation were better distributed over the whole electrode surface, preventing the formation of areas with low electric current densities and increasing the electroactive area used for metallic deposition.

References

Berube J.R.R., Babiec S., Phillip-Jameson J., Negele A.R. & Willis M.J. (1990) Calcined kaolin clay filler pigment enhances opacity and printing properties of newsprint and mechanical papers. US Patent No. US5011534A, 1990-02-14. Retrieved from https://patents.google.com/patent/US5011534A (accessed 1 March 2022).

Bisang J.M. & Kreysa G. (1988) Study the effect of electrode resistance on current density distribution in cylindrical electrochemical reactors. *Journal of Applied Electrochemistry*, **18**, 422–430.

Bloodworth A.J., Highley D.E. & Mitchell C.J. (1993) *Industrial Minerals Laboratory Manual KAOLIN*. British Geological Survey, Nottingham, UK, 80 pp.

Chen Y., Zhou C., Alshameri A., Zhou S., Ma Y., Sun T. & Yan C. (2014) Effect of rice hulls additions and calcination conditions on the whiteness of kaolin. *Ceramics International*, **40**, 11751–11758.

Cullivan J., Williams R. & Cross R. (2003) Understanding the hydrocyclone separator through computational fluid dynamics. *Chemical Engineering Research and Design*, **81**, 455–466.

Flores-Segura J.C., Reyes-Cruz V.E., Legorreta-Garcìa F., Hernández-Cruz L. & Veloz-Rodríguez M. (2012) Purification of kaolin clays employing electrochemical techniques. Pp. 145–154 in: *Recent Developments in Metallurgy, Materials, and Environment* (M.I. Pech-Canul, A.L. Leal Cruz, J.C. Rendón Angeles & C.A. Gutiérrez, editors). CINVESTAV IPN, Mexico City, Mexico.

Flores-Segura J.C., Savadogo O., Oishi K., Reyes-Cruz V.E. & Veloz-Rodríguez M.A. (2016) Electrodeposition of iron from kaolin clay and the effect of mass transport. *Journal of New Materials for Electrochemical Systems*, **19**, 103–107.

Flores-Segura J.C., Reyes-Cruz V.E., Pérez-Bueno J.D., Lozada-Ascencio E.M. & Legorreta-García F. (2017) Characterization and electrochemical treatment of kaolin. *Applied Clay Science*, **146**, 264–269.

Forbus E.S., Gantt G.E., Willis M.J. & Young R.H. (1993) European Patent No. EP0693043A1. 1993-04-06. Retrieved from https://patents.google.com/patent/EP0693043A1 (accessed 1 March 2022).

González J. & Ruiz M. (2006) Bleaching of kaolins and clays by chlorination of iron and titanium. *Applied Clay Science*, **33**, 219–229.

Hernández-Hernández R.A., Legorreta-García F., Hernández-Cruz L.E. & Bedolla-Jacuinde A. (2015) Kaolin bleaching by leaching using phosphoric acid solutions. *Journal of the Mexican Chemical Society*, **59**, 198–202.

Houghton R.W. & Kuhn T. (1974) Mass-transport problems and some design concepts of electrochemical reactors. *Journal of Applied Electrochemistry*, **4**, 173–190.

Langenbeck K. (1908) US Patent No. US893590. 1907-09-17. Retrieved from https://patents.google.com/patent/US893590A (accessed 1 March 2022).

Lee J. & Selman J.R. (1982) Effects of separator and terminal on the current distribution in parallel-plate electrochemical flow reactors. *Journal of Electrochemical Society*, **129**, 1670–1678.

Li Y. (2014) CN Patent No. CN104030307B. 2014-05-16. Retrieved from https://patents.google.com/patent/CN104030307B (accessed 1 March 2022).

Li S. (2017) Introduction to electrochemical reaction engineering. Pp. 599–651 in: *Reaction Engineering*. Butterworth-Heinemann, Oxford, UK.

Li H., Jiao X. & Zhou J. (2013) The present status and the prospect of research on kaolin's de-ironing and bleaching technology. *Journal of Advances in Chemistry*, **2**, 42–49.

Lim E.C.L., Chen Y.-R., Wang C.-H. & Wu R.-M. (2010) Experimental and computational studies of multiphase hydrodynamics in a hydrocyclone separator system. *Chemical Engineering Science*, **65**, 6415–6424.

Liu Z., Wainright J., Huang W. & Savinella R. (2004) Positioning the reference electrode in proton exchange membrane fuel cells: calculations of primary and secondary current distribution. *Electrochimica Acta*, **49**, 923–935.

Low C., Roberts E. & Walsh F. (2007) Numerical simulation of the current, potential and concentration distributions along the cathode of a rotating cylinder hull cell. *Electrochimica Acta*, **52**, 3831–3840.

Lu X., Zhu Y., Jiang R., Huang Y. & Jiang G. (2006) Research on removal of iron and titanium from kaolin by electrochemical method. *Journal of China University of Mining & Technology*, **3**, 254–258.

Ma S. & Li F. (2006) Experimental study on the purifying bleaching kaolin fine tailings with organic acids. *Inorganic Chemicals Industry*, 10. Retrieved from http://en.cnki.com.cn/Article_en/CJFDTotal-WJYG200610008.htm (accessed 1 March 2022).

Maynard J., Millman N. & Iannicelli J. (1969) A method for removing titanium dioxide impurities from kaolin. *Clays and Clay Minerals*, **17**, 59–62.

Melo-López A.A., Veloz-Rodríguez M., Reyes-Cruz V., Urbano-Reyes G., Cobos-Murcia J. & Legorreta-García F. (2018) Electrochemical purification of kaolinitic for removing Fe and Ti oxides applying an ultrasonic pretreatment. *Applied Clay Science*, **162**, 461–468.

https://doi.org/10.1180/clm.2022.36 Published online by Cambridge University Press

Nadebaum P. & Fahidy T.Z. (1980) Design of electrochemical reactors *via* a sequential factorial costing technique. *Journal of Applied Electrochemistry*, **10**, 13–24.

Okada H., Mitsuhashi K., Ohara T., Whitby E.R. & Wada H. (2007) Computational fluid dynamics simulation of high gradient magnetic separation. *Separation Science and Technology*, **40**, 1567–1584.

Panzhong W., Tao Z., Haiman X. & Jingsi Y. (2010) Study on de-ironing and bleaching process of kaolin. *China Powder Science and Technology*, 3. Retrieved from http://en.cnki.com.cn/Article_en/CJFDTotal-FTJS201003022.htm (accessed 1 March 2022).

Pentrák M., Madejová J. & Komadel P. (2018) Acid and alkali treatment of kaolins. *Clay Minerals*, **44**, 511–523.

Pérez T., Ponce de León C., Walsh F. & Nava Montes de Oca J. (2015) Simulation of current distribution along a planar electrode under turbulent flow conditions in a laboratory filter-press flow cell. *Electrochimica Acta*, **154**, 352–360.

Raghavan P., Chandrasekhar S., Vogt V. & Gock E. (2004) Separation of titaniferous impurities from kaolin by high shear pretreatment and froth flotation. *Applied Clay Science*, **25**, 110–120.

Reyes-Cruz V.E. & Flores-Segura J.C. (2015) MX Patent No. MX/E/2015/035230, 2016-10-31. Retrieved from https://worldwide.espacenet.com/publicationDetails/originalDocument?CC=MX&NR=2015006239A&KC=A&FT=D&ND=4&date=20161031&DB=EPODOC&locale=en_EP (accessed 1 March 2022).

Reyes-Cruz V.E., Cobos-Murcia J.A., Veloz-Rodríguez M.A.-G., Melo-López A.A. & García-Hernández V. (2017) MX Patent No. MX/E/2017/092353. Retrieved from https://worldwide.espacenet.com/publicationDetails/originalDocument?CC=MX&NR=2017016144A&KC=A&FT=D&ND=3&date=20190524&DB=EPODOC&locale=en_EP (accessed 1 March 2022).

Rodríguez-Morales E., Montes-Rodríguez J., Luna-Bustamante A., Balderas-Puga D. & Luna-González C. (2020) Numerical study of carburizing and quenching thermochemical treatment of a drive shaft employing experiment design. *Revista Mexicana de Ingeniería Química*, **14**, 405–413.

Shelobolina E., Pickering S. & Lovley D. (2005) Fe-cycle bacteria from industrial clays mined in Georgia, USA. *Clays and Clay Minerals*, **53**, 580–586.

Shengwu Y., Yujuan X., Jiang-feng L., Baojun Y., Yan Y. & Bainian W. (2012) CN Patent No. CN102583412A. Retrieved from https://patents.google.com/patent/CN102583412A/ko (accessed 1 March 2022).

Sulaymon A.H. & Abbar A.H. (2012) Scale-up of electrochemical reactors. Chapter 9 in: *Electrolysis* (J. Kleperis & V. Linkov, editors). Intech Open, London, UK.

Teklay A., Yin C. & Rosendahl L. (2016) Flash calcination of kaolinite rich clay and impact of process conditions on the quality of the calcines: a way to reduce CO_2 footprint from cement industry. *Applied Energy*, **162**, 1218–1224.

Thompson T.D. (1982) US Patent No. US4451440A. Retrieved from https://patents.google.com/patent/US4451440A (accessed 1 March 2022).

Vázquez A., Rodríguez I. & Lázaro I. (2012) Primary potential and current density distribution analysis: a first approach for designing electrocoagulation reactors. *Chemical Engineering Journal*, **179**, 253–261.

Walsh F. & Reade G. (1994) Design and performance of electrochemical reactors for efficient synthesis and environmental treatment. Part 1. Electrode geometry and figures of merit. *Analyst*, **119**, 791–796.

Wang Z., Li H., Chen H., Lv J., Leng H., Xiao J. & Wang S. (2021) Effects of grinding and dehydration on kaolin in a steam jet mill. *Clay Minerals*, **56**, 75–84.

White R.E., Bain M. & Raible M. (1983) Parallel plate electrochemical reactor model. *Journal of Electrochemical Society*, **130**, 1037–1042.

Yijun Y., Bin L. & Jing S. (2012) CN Patent No. CN102874826B. Retrieved from https://patents.google.com/patent/CN102874826B (accessed 1 March 2022).

Yildirim I., Pruett R.J. & Meizanis P.M. (2012) US Patent No. US20150259857A1. Retrieved from https://patents.google.com/patent/US20150259857A1 (accessed 1 March 2022).

Yin Y. & Huang Q. (2013) CN Patent No. CN103666008B. Retrieved from https://patents.google.com/patent/CN103666008B (accessed 1 March 2022).

Yishui S (1989) Bleaching technology for removing iron by kaolin. CN Patent No. CN1041739A. Retrieved from https://worldwide.espacenet.com/patent/search/family/004857391/publication/CN1041739A?q=pn%3DCN1041739A (accessed 1 March 2022).

Yustres A., López-Vizcaíno R., Sáez C., Cañizares P., Rodrigo M. & Navarro V. (2018) Water transport in electrokinetic remediation of unsaturated kaolinite. Experimental and numerical study. *Separation and Purification Technology*, **192**, 196–204.

https://doi.org/10.1180/clm.2022.36 Published online by Cambridge University Press